Microstructural characteristics and carbide transformation of laser-cladded Fe-Cr-W-Ni-C coatings during high-temperature tempering

XIAOLEI WU, GUANGNAN CHEN
Materials Research Center, Institute of Mechanics, Chinese Academy of Sciences, 15 ZhongGuanCun Rd, Beijing 100080, People's Republic of China
E-mail: xlwu@cc5.imech.ac.cn

Laser-cladding is the process of producing metallurgically well-bonded coatings of a great variety of materials. With high-speed cladding, extremely fine and homogenous microstructures, characteristic of rapid processes, can be obtained. The hard and resistant laser-cladded iron-based coatings widely studied at present are Fe-ΣX-C (X = Cr, Mn, W, B, etc.) systems [1–3]. Although the microstructural modification of Fe-based alloys by laser-cladding with various compositions and process parameters has been demonstrated, only a small amount of atttention has been given to the microstructural characteristics and transformations of non-equilibrium and meta-stable phases, especially at elevated temperatures that control the mechanical properties of the coating. There is, therefore, a need for understanding the microstructural evolution of the clad coating during tempering.

The coating alloy is a powder mixture of Fe, Cr, W, Ni, and C with a weight ratio of 10:5:1:1:1. The substrate material is 5CrMnMo, in a quenched and tempered condition. Clad is carried out with a continuous wave 3 kW CO_2, laser equipped with a powder delivery system and an argon gas-guidance device. The clad parameters are process speed of 17 mm/s, laser beam of 2 mm diameter, laser power of 2 kW, and feed rate of 0.35 g/s. The as-solidified microstructures and phase transitions during tempering at 923 K for 2 h were analyzed by analytical transmission electron microscopy. Fig. 1 shows the TEM micrographs of the coating. The primary phase of solidification was determined to be austenite, γ_e

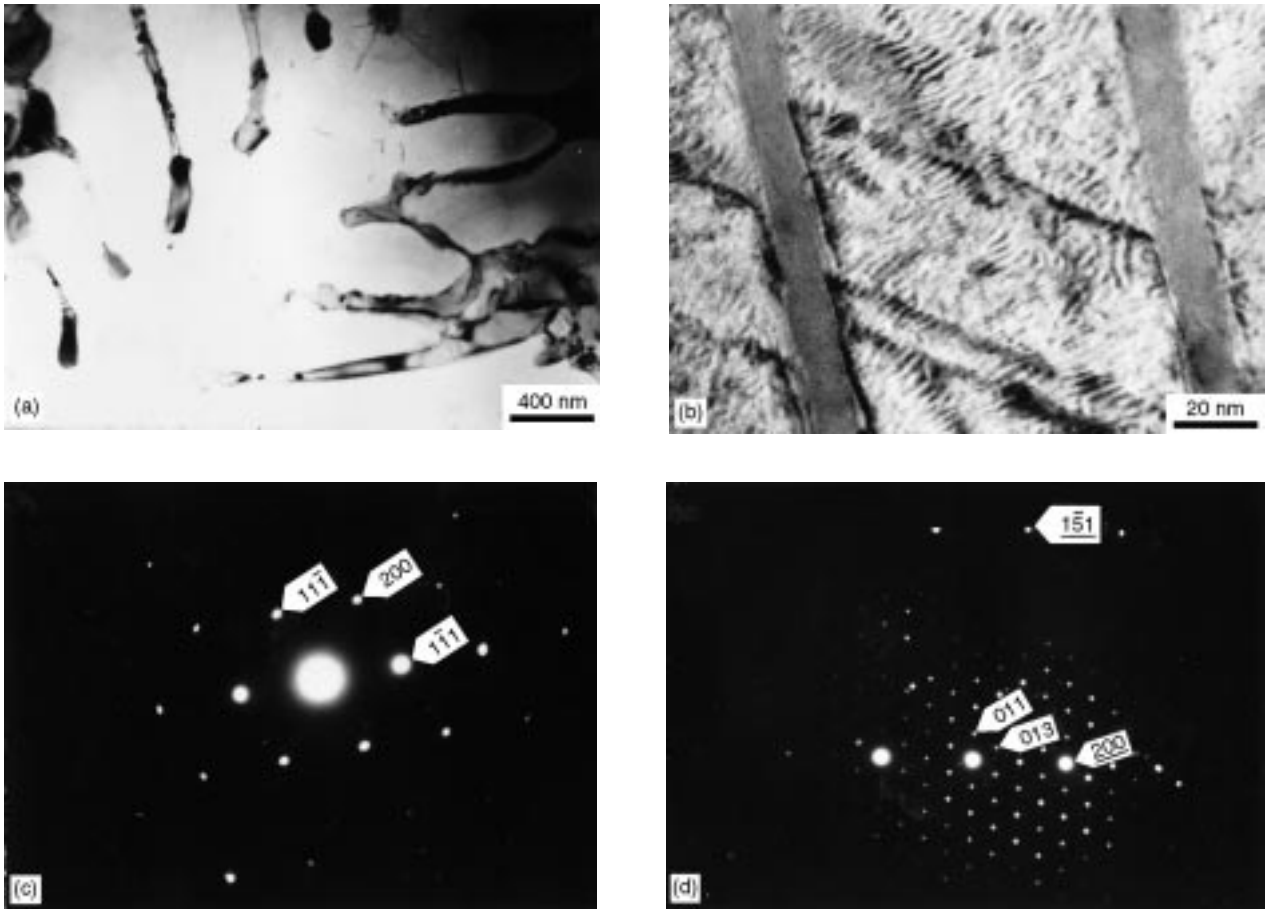

Figure 1 Bright-field TEM micrographs, showing microstructures of the clad coatings: (a) primary austenite with a dendrite morphology; (b) interdendritic lamellar eutectic, consisting of ($\gamma + M_7C_3$); (c) diffraction pattern of the primary austenite in (a); (d) selected area diffraction pattern covering an M_7C_3 and surrounding austenite in (b) (hkl:austenite, hkl:carbide).

0261-8028

with a dendritic morphology, as shown in Fig. 1a. Fig. 1b is a bright-field TEM micrograph, revealing an interdendritic lamellar eutectic composed of austenite, γ_d, and hexagonal M_7C_3 (M = Cr, Fe, W, Ni) carbides. Fig. 1c is a diffraction pattern, with indexing taken from the primary austenite of Fig. 1a. Fig. 1d is a selected area diffraction pattern with indexing taken from an area covering an M_7C_3 and surrounding the austenite of Fig. 1b. The diffraction pattern of plate-like M_7C_3 carbides with a dark contrast shows a characteristic six-fold symmetry, and the unit cell dimensions of crystal structure are $a_0 = 1.387$ nm and $c_0 = 0.496$ nm. Thus, the microstructure is of hypoeutectic feature, i.e., $\gamma_e + (\gamma_d + M_7C_3)$. The experimental result is consistent with the previous study [3]. M_7C_3 is a meta-stable phase and its decomposition temperature is about 873 K [4]. Thus, the dissolution and transformation of M_7C_3 may occur during high-temperature tempering.

Fig. 2a shows an *in situ* transformation of $M_{23}C_6$ from M_7C_3 carbides. Granular $M_{23}C_6$ carbides may form directly inside M_7C_3 or at the M_7C_3/austenite interface. A lot of $M_{23}C_6$ carbides also precipitate within austenite. Fig. 2b is a selected area diffraction pattern with indexing taken from an area covering M_7C_3, $M_{23}C_6$ and the surrounding austenite.

Figs 3a and b are bright- and dark-field TEM micrographs, illustrating plate-like $M_{23}C_6$ carbides with twin substructures precipitated from eutectic austenite. Fig. 3c is a diffraction pattern with

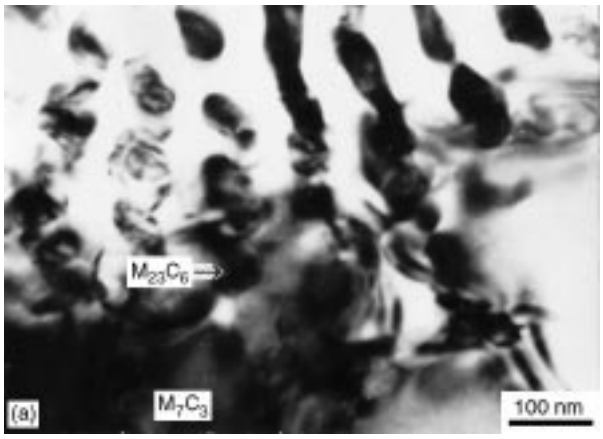

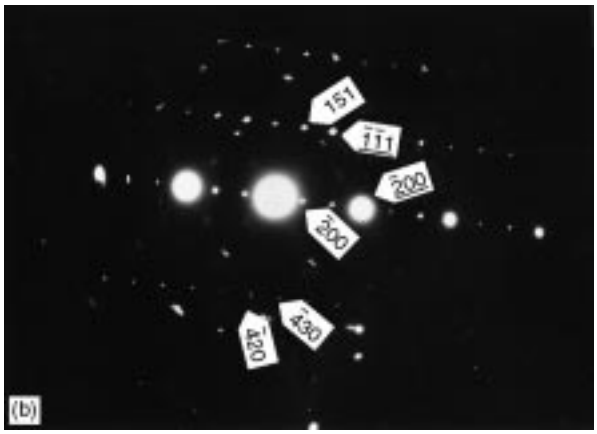

Figure 2 TEM micrograph indicating an *in situ* transformation of $M_7C_3 \rightarrow M_{23}C_6$: (a) bright-field image showing granular $M_{23}C_6$ either nucleated at M_7C_3/γ interface, inside M_7C_3, or precipitated in eutectic austenite; (b) selected area diffraction pattern taken from an area covering an M_7C_3, $M_{23}C_6$ and surrounding austenite (hkl:austenite, hkl:M_7C_3, hkl:$M_{23}C_6$).

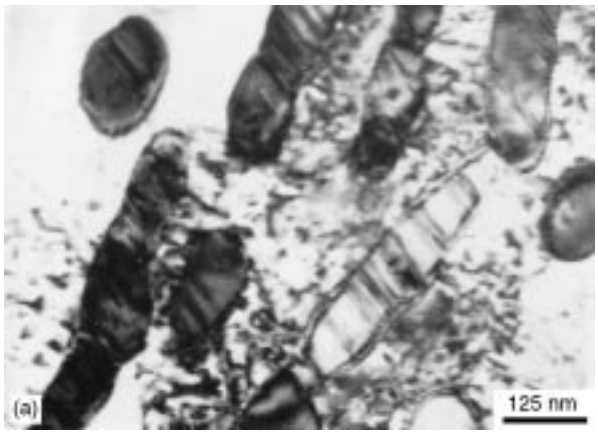

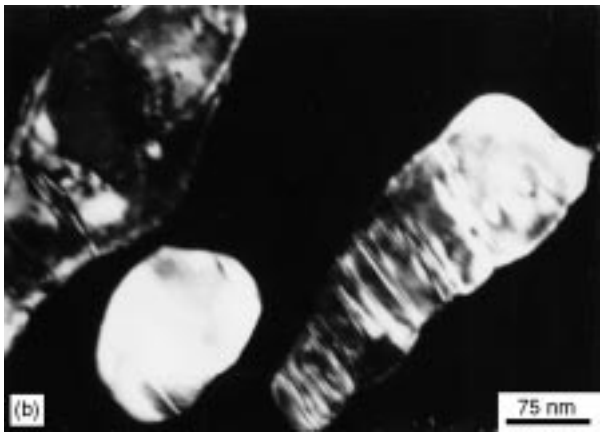

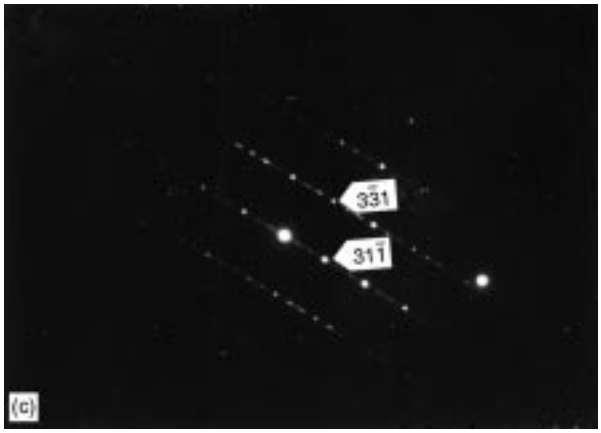

Figure 3 TEM micrographs, showing morphologies and fine structures of plate-like $M_{23}C_6$ carbides: (a) heterogeneously precipitated from eutectic austenite; (b) bright- and dark-field images; (c) selected area diffraction pattern with indexing taken from an area covering an $M_{23}C_6$.

indexing taken from a $M_{23}C_6$ carbide. Both *in situ*-transformed (Fig. 2a) and precipitated (Fig. 3a) $M_{23}C_6$ carbides are determined to be Cr-Fe-rich carbides by using EDAX.

Figs 4a and b reveal bright-field TEM micrographs of small fibrous and plate-like M_2C carbides precipitated from γ_e and γ_d, respectively. They are determined to be W_2C carbides by composition analyses.

Fig. 5 shows TEM micrographs that demonstrate an *in situ* transformation of $M_7C_3 \rightarrow M_6C$. The long plate-like and larger granular carbides, both with a light black contrast, are M_7C_3 in Figs 5a and b. Very fine granular carbides with a dark black contrast are M_6C. Fig. 5c is the diffraction pattern of M_7C_3, with indexing in Fig. 5a. Fig. 5d is a select area diffraction pattern, taken from an area covering an M_6C and the surrounding austenite in Fig. 5a. The distinction between M_6C and $M_{23}C_6$ is difficult because both structures are based on the same fcc bravais lattice, with very close sizes of unit cell, 1.113 nm and 1.086 nm, respectively. However, M_6C

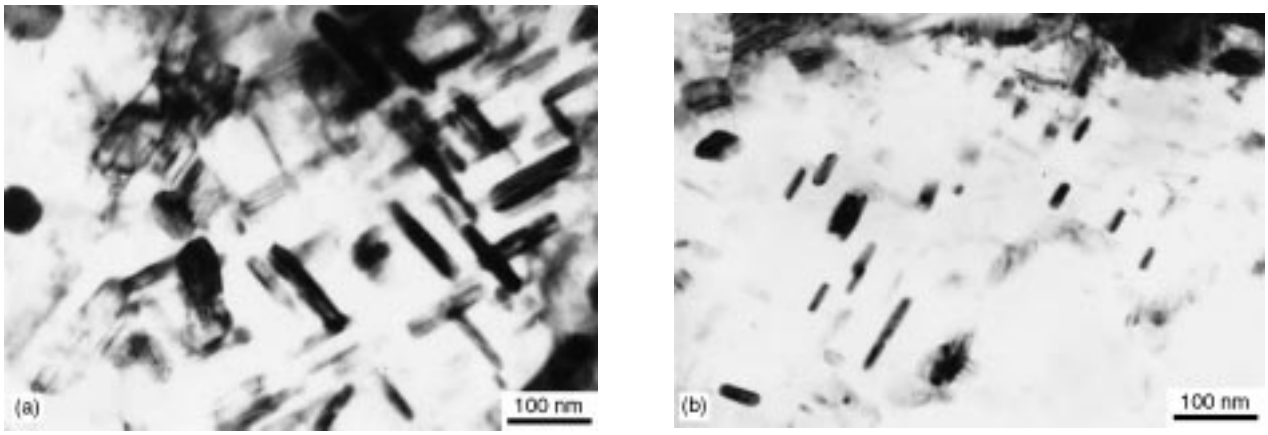

Figure 4 Bright-field TEM micrographs: (a) indicating M_2C precipitated from eutectic austenite; (b) dendrite austenite.

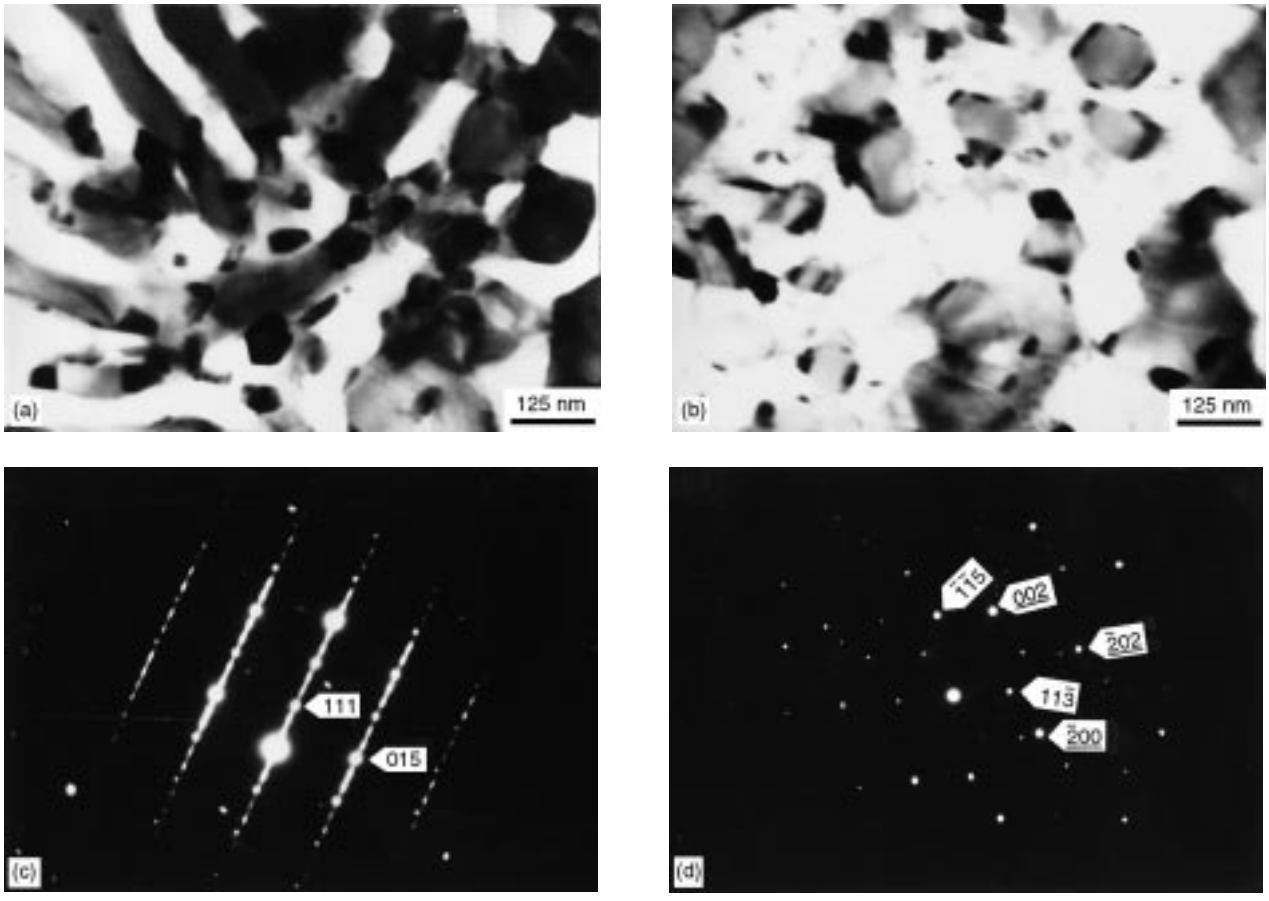

Figure 5 TEM micrographs showing an *in situ* transformation of $M_7C_3 \rightarrow M_6C$: (a) and (b) bright-field images of M_6C nucleated at the M_7C_3/γ interface in lamellar and honeycomb eutectic, respectively. Granular M_6C is with a deep black contrast, M_7C_3 is with light black contrast, and γ is with white contrast; (c) diffraction pattern taken from an area covering an M_7C_3 of (a); (d) selected area diffraction pattern taken from an area covering an M_6C and surrounding austenite of (a) (hkl:ferrite, hkl:carbide).

and $M_{23}C_6$ belong to Fd3m and Fm3m space groups respectively [5]. Also M_6C and $M_{23}C_6$ are W-rich and Cr-Fe-rich carbides, respectively. Thus, it is easy to discriminate one from the other by using the extinction rules for the different space groups or by analysis of element compositions.

The precipitation and *in situ* transition of alloy carbides have been widely studied in conventionally treated steels by many authors [6–8]. The evidence for the *in situ* transformation sequency $M_7C_3 \rightarrow M_6C$ was established in chromium alloyed steels [7]. The *in situ* transition has been observed for the reaction of $M_7C_3 \rightarrow M_{23}C_6$ [8]. As for microstructures by laser *in situ* syntheses of ferrous coatings, however, there mainly exist non-equilbrium phases, such as austenite with extended solid solution to a large scale, and meta-stable phases, the transition and evolution of which have not been established, especially during high temperature tempering.

In conclusion, the hypoeutectic microstructure, i.e., the primary austenite and $(\gamma + M_7C_3)$ eutectic, is obtained by laser clad Fe-Cr-W-Ni-C alloys at present process conditions. The heterogeneous precipitation of $M_{23}C_6$ and M_2C in austenite and *in situ* homogeneous transformation of $M_7C_3 \rightarrow M_{23}C_6$ and $M_7C_3 \rightarrow M_6C$ occur during high-temperature tempering at 923 K for 2 h.

Acknowledgments

This research was supported by National Natural Science Foundation of China, No. 59836220, Major Research Foundation of Chinese Academy of Sciences, No. KY951-A1-601-03, and Postdoctor Research Foundation of China, No. 4868.

References

1. W. M. STEEN, "Surface Treatment and Film Deposition", edited by J. Mazumder, O. Conde, R. Villar and W. Steen, NATO ASI Series E, *Applied Sciences* **307** (1996) 1.
2. J. SINGH and J. MAZUMDER, *Metall. Trans. A* **18A** (1987) 313.
3. K. NAGARATHNAM and K. KOMVOPOULOS, *Metall. Mater. Trans. A* **24A** (1993) 1621.
4. J. P. MORNIROLI, E. BAUER-GROSSE and M. GANTOIS, *Philos. Mag. A* **48** (1983) 311.
5. P. B. HIRSCH, A. HOWIE, R. B. NICHOLSON, D. W. PASHLEY and M. J. WHELAN, "Electron Microscopy of Thin Crystals" (Krieger, New York, USA, 1977) p. 91.
6. D. V. SHTANSKY and G. INDEN, *Acta Mater.* **45** (1997) 2861.
7. V. G. RIVLIN, *Inter. Metals Rev.* **30** (1985) 104.
8. V. J. RAGHAVAN, *Phase Equil.* **15** (1994) 425.

Received 28 March
and accepted 15 July 1998